powders

MDPI

Article

Effect of Carbon Nanotube Addition on Densification Behavior, Activation Energy, and Microstructural Evolution of WC-Co Cemented Carbides

José Luis Cabezas-Villa, Victor Sayil López-Álvarez, Gustavo Castro-Sánchez and José Lemus-Ruiz *

Instituto de Investigación en Metalurgia y Materiales (IIMM), Universidad Michoacana de San Nicolás de Hidalgo (UMSNH), Morelia 58030, Michoacán, Mexico; luis.cabezas@umich.mx (J.L.C.-V.); victor.lopez.alvarez@umich.mx (V.S.L.-Á.); gustavo_yx@hotmail.com (G.C.-S.)

* Correspondence: jlruiz@umich.mx

Abstract

This study investigates the effect of carbon nanotube (CNT) addition on the densification behavior, activation energy, microstructural evolution, and mechanical performance of WC-Co cemented carbides processed by liquid-phase sintering. WC-Co and WC-Co reinforced with 5 vol.% CNT were fabricated by powder metallurgy and sintered under argon atmosphere at temperatures between 1380 and 1400 °C using different holding times. Relative density measurements, dilatometric analysis, scanning electron microscopy, and Vickers hardness and fracture toughness evaluations were performed to assess the influence of CNT incorporation on the sintering response and resulting microstructure. The results showed that increasing sintering temperature and holding time promoted densification and microstructural consolidation in both systems. Although CNT addition slightly reduced the final relative density, it promoted a finer and more homogeneous carbide distribution. Dilatometric analysis revealed that CNT incorporation modified the densification kinetics and increased the apparent activation energy from 99.36 ± 8 kJ/mol for WC-Co to 126.47 kJ/mol for WC-Co + 5 vol.% CNT, corresponding to an increase of approximately 27%, indicating significant changes in the diffusion-controlled mass transport mechanisms governing liquid-phase sintering. Furthermore, the CNT-reinforced material exhibited improved mechanical performance, reaching hardness and fracture toughness values of approximately 1090 kgf/mm^2 and 10.5 MPa·m$^{1/2}$, respectively, compared with 995 kgf/mm^2 and 8.6 MPa·m$^{1/2}$ for the unreinforced WC-Co system. Enhanced fracture resistance was further supported by reduced crack propagation after Vickers indentation. The results demonstrate that CNT incorporation acts not only as a reinforcing phase but also as a microstructural and kinetic modifier, providing an effective strategy for controlling densification behavior and improving the performance of WC-Co cemented carbides processed by liquid-phase sintering.

Keywords: WC-Co cemented carbides; carbon nanotubes; liquid-phase sintering; densification behavior; activation energy; microstructural evolution

Check for updates

Academic Editor: Paul F. Luckham

Received: 17 June 2026
Revised: 16 July 2026
Accepted: 30 July 2026
Published: 4 August 2026

Copyright: © 2026 by the authors. Licensee MDPI, Basel, Switzerland. This article is an open access article distributed under the terms and conditions of the Creative Commons Attribution (CC BY) license.

1. Introduction

WC-Co cemented carbides are widely used in cutting tools, wear-resistant components, mining applications, and high-performance engineering systems due to their excellent combination of hardness, strength, and wear resistance [1,2]. The mechanical performance of these materials strongly depends on their microstructural characteristics, particularly

carbide grain size, binder phase distribution, porosity, and densification achieved during liquid-phase sintering [3,4]. Consequently, the control of sintering conditions and microstructural evolution remains a critical aspect in the processing of cemented carbides. During liquid-phase sintering of WC-Co systems, densification and grain growth occur simultaneously through diffusion-assisted mechanisms involving dissolution and reprecipitation processes in the cobalt-rich liquid phase [4–6]. Although increasing sintering temperature and holding time generally promotes densification, excessive grain coarsening may negatively affect hardness, fracture toughness, and overall mechanical performance [7,8]. Therefore, several studies have focused on developing alternative approaches to control grain growth and improve microstructural stability during sintering [9].

In recent years, carbon nanotubes (CNTs) have attracted considerable attention as reinforcing agents in metal matrix composites and cemented carbide systems due to their exceptional mechanical properties, high aspect ratio, thermal stability, and potential ability to modify diffusion and grain growth behavior during thermal processing [10,11]. The incorporation of CNTs into WC-Co systems has been associated with grain refinement and improvements in hardness and fracture toughness [12,13]. However, achieving homogeneous CNT dispersion and understanding their influence on densification mechanisms and sintering behavior remain significant challenges [14]. Several studies have reported the beneficial effects of CNT incorporation on the microstructural and mechanical properties of cemented carbides; however, the influence of CNTs on densification kinetics during liquid-phase sintering remains insufficiently understood [15,16].

In particular, limited information is available regarding the combined relationship between CNT addition, dilatometric behavior, activation energy, microstructural evolution, and the resulting mechanical performance of WC-Co cemented carbides [12,17,18]. Since densification, grain growth, and microstructural development are strongly dependent on diffusion-controlled processes, a better understanding of the kinetic effects associated with CNT incorporation is required. Furthermore, only a limited number of studies have investigated the relationships among densification behavior, dilatometric response, activation energy, microstructural evolution, and mechanical performance in WC-Co-based systems, particularly when CNT reinforcement is involved [4,14,19]. Consequently, the mechanisms by which CNTs influence densification behavior and microstructural development during liquid-phase sintering remain topics of considerable scientific and technological interest.

Therefore, the present work investigates the effect of carbon nanotube addition on the densification behavior, microstructural evolution, sintering kinetics, activation energy, and mechanical performance of WC-Co cemented carbides processed by powder metallurgy and liquid-phase sintering. Dilatometric analysis was employed to evaluate shrinkage behavior and diffusion-related mechanisms at different heating rates, while scanning electron microscopy was used to analyze the resulting microstructural changes after sintering. The relationship between sintering kinetics, activation energy, microstructural evolution, and mechanical properties is discussed in order to provide further insight into the mechanisms governing densification, microstructural evolution, and mechanical performance in CNT-reinforced WC-Co cemented carbides processed by liquid-phase sintering.

2. Experimental Procedure

2.1. Raw Materials

Commercial WC-Co powder containing 6 wt.% Co (WC-6Co) supplied by Atlantic Equipment Engineers (AEE, Upper Saddle River, NJ, USA) was used as the matrix material in this study. Carbon nanotubes (CNTs) synthesized by spray pyrolysis chemical vapor deposition using alpha-pinene as carbon source and ferrocene as catalyst precursor were

employed as reinforcement [20]. After synthesis, the CNTs were purified and functionalized to improve their dispersion within the WC-Co matrix. A CNT content of 5 vol.% was selected to evaluate its influence on densification behavior, microstructural evolution, sintering kinetics, activation energy, and mechanical performance during liquid-phase sintering. Further details regarding CNT synthesis and functionalization are provided in Section 2.2.

2.2. CNT Synthesis and Functionalization

Carbon nanotubes (CNTs) were synthesized through a spray pyrolysis chemical vapor deposition process using alpha-pinene as carbon precursor and ferrocene as catalyst precursor under argon atmosphere at 700 °C [21]. After synthesis, the CNTs were purified by acid treatment in nitric acid in order to remove catalyst residues and amorphous carbon. Subsequently, the purified CNTs were functionalized using a HNO_3/H_2SO_4 solution to improve their dispersion and interfacial interaction with the WC-Co matrix [22,23]. The functionalized CNTs were filtered, washed with distilled water until neutral pH, and dried prior to powder processing.

2.3. Powder Processing and Mixing

Prior to powder processing, the functionalized CNTs were dispersed in isopropyl alcohol and ultrasonically agitated for 15 min in order to reduce agglomeration and improve their distribution within the WC-Co matrix [24]. The resulting suspension was subsequently dried at 80 °C before powder mixing. The WC-Co powder and CNTs were mechanically mixed in a 3-inch ceramic milling jar using a ball mill operated at 180 rpm for 4 h. High-purity yttria balls with a diameter of ¼ inch were employed as grinding media to promote homogeneous mixing of the powder constituents. After milling, the resulting powder mixtures were dried and prepared for compaction and subsequent liquid-phase sintering.

2.4. Compaction and Sintering

The powder mixtures were uniaxially compacted at 200 MPa using a cylindrical steel die to produce green compacts with dimensions of approximately 6.3 mm in diameter and 3 mm in height. The compacts were subsequently sintered in a Carbolite STF 16/180 horizontal tube resistance furnace (Carbolite, Hope Valley, Derbyshire, UK) under argon atmosphere. Liquid-phase sintering was carried out at temperatures of 1380 °C and 1400 °C using holding times of 30 and 60 min. The furnace was heated at a constant heating rate of 20 °C/min until the selected sintering temperatures were reached. The same processing conditions were applied to both the unreinforced WC-Co and WC-Co + 5 vol.% CNT systems to enable a direct comparison of the effects of CNT incorporation on densification behavior, microstructural evolution, sintering kinetics, activation energy, and mechanical performance. The selected sintering temperatures and holding times were chosen to represent typical liquid-phase sintering conditions for WC–Co cemented carbides reported in the literature [25] and to evaluate their combined effect on densification behavior, microstructural evolution, sintering kinetics, activation energy, and mechanical performance. The present experimental design was intended to investigate representative processing conditions rather than to isolate the individual contribution of each processing parameter. After sintering, all specimens were furnace cooled under argon prior to characterization. The synthesis, purification, mixing, compaction, sintering, and characterization stages employed in this work are schematically illustrated in Figure 1.

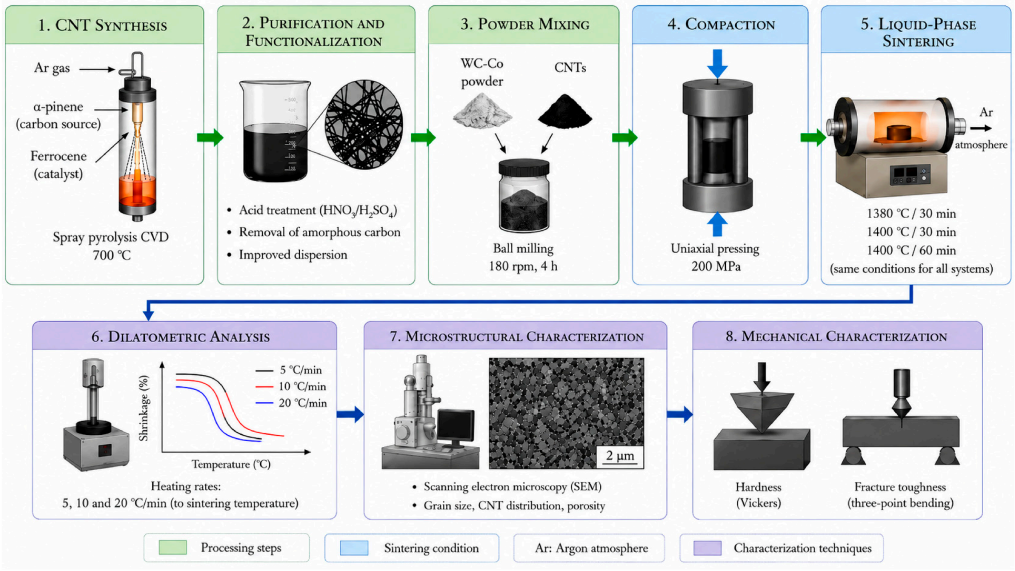


Figure 1. Schematic illustration of the experimental procedure used for the processing and characterization of CNT-reinforced WC-Co cemented carbides.

2.5. Dilatometric Analysis

Dilatometric experiments were carried out using a vertical Linseis L75V dilatometer (LINSEIS Messgeräte GmbH, Selb, Germany) in order to evaluate the sintering kinetics and densification behavior of WC-Co and CNT-reinforced systems. Cylindrical compacts with dimensions of approximately 6.3 mm in diameter and 3 mm in height were prepared under the same compaction conditions previously described. The dilatometric analysis was performed under argon atmosphere using controlled heating rates of 5, 10, and 20 °C/min. The WC-Co series was recorded up to 1260 °C because of the upper-temperature capability available during those measurements, whereas the WC-Co + 5 vol.% CNT series was subsequently recorded up to 1420 °C after instrument servicing restored the extended temperature range. Axial dimensional changes during heating were continuously recorded with a precision of ±0.1 µm. The obtained shrinkage curves were used to analyze densification behavior during solid-state and liquid-phase sintering. Although the dilatometric experiments were conducted up to a maximum temperature of 1420 °C, only the temperature range containing measurable densification is presented, since no significant dimensional changes were observed beyond this region. In addition, the apparent activation energy associated with the densification process was estimated from dilatometric data acquired at different heating rates using an Arrhenius-type approach [19,26].

2.6. Microstructural Characterization

The sintered samples were characterized by scanning electron microscopy (SEM) in order to evaluate microstructural evolution, porosity distribution, and fracture characteristics after sintering [25,27]. Fractured and polished surfaces were analyzed under different magnifications to identify the effect of CNT addition on the resulting WC-Co microstructure.

2.7. Mechanical Characterization

Vickers hardness and fracture toughness measurements were performed on selected sintered samples in order to evaluate the effect of CNT addition on the mechanical response of the WC-Co systems. Hardness tests were carried out using a Vickers indenter under a load of 30 kgf. Fracture toughness values were estimated from the cracks generated around the Vickers indent using the indentation fracture (IF) method [28,29].

3. Results and Discussion

3.1. Densification Behavior of WC-Co Systems

The relative density values obtained for WC-Co and CNT-reinforced WC-Co systems processed under different liquid-phase sintering conditions are presented in Figure 2. In general, densification increased with increasing sintering temperature and holding time for both systems, indicating enhanced mass transport, particle rearrangement, and consolidation during liquid-phase sintering. As shown in Figure 2, the WC-Co system exhibited relative density values ranging from 71.3% to 83.1%, while the WC-Co + 5 vol.% CNT system reached values between 70.8% and 82.2%. Under equivalent sintering conditions, the CNT-containing samples consistently exhibited slightly lower relative density values than the unreinforced WC-Co system. The difference in relative density was approximately 0.5% at 1380 °C for 30 min, 3.0% at 1400 °C for 30 min, and 0.9% at 1400 °C for 60 min. Nevertheless, both systems showed a progressive increase in relative density with increasing sintering severity, indicating that the incorporation of CNTs did not significantly hinder the overall densification process.

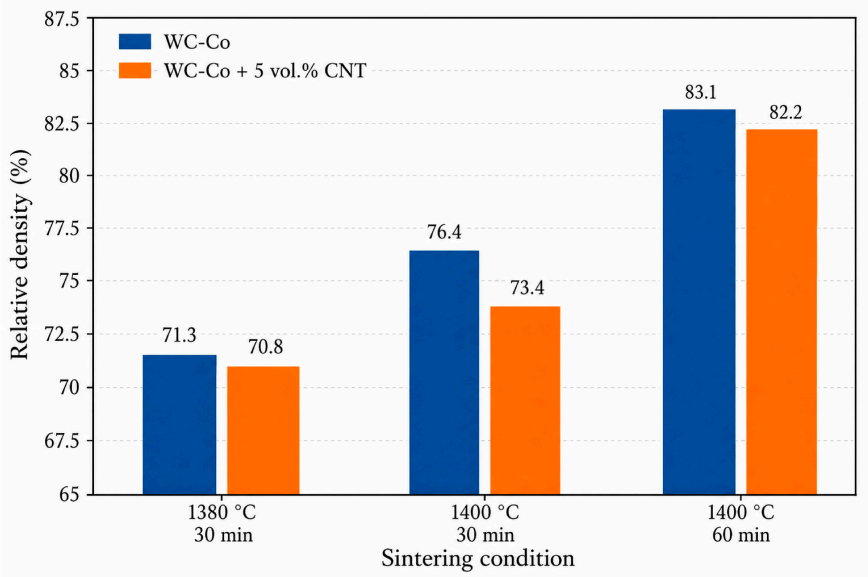


Figure 2. Relative density of WC-Co and CNT-reinforced WC-Co systems sintered under different temperature and holding time conditions.

The highest relative density values were obtained at 1400 °C for 60 min, reaching 83.1% for WC-Co and 82.2% for WC-Co + 5 vol.% CNT. These results suggest that the selected processing conditions promoted effective liquid-phase sintering and particle rearrangement mechanisms, leading to improved consolidation of the cemented carbide systems [30]. The progressive increase in relative density observed with increasing temperature and holding time is consistent with the activation of liquid-phase-assisted densification mechanisms. During liquid-phase sintering, the cobalt-rich liquid phase promotes particle rearrangement, pore elimination, and dissolution–reprecipitation processes, which contribute to enhanced densification of WC-Co systems [30–32]. The formation of a liquid binder phase improves capillary-driven accommodation of particles and facilitates mass transport between tungsten carbide grains. The experimental design adopted in this study was intended to evaluate representative liquid-phase sintering conditions by simultaneously varying temperature and holding time rather than independently assessing the individual contribution of each processing parameter. Nevertheless, the experimental results indicate that increasing sintering temperature produced the most pronounced improvement in densification by promoting liquid-phase formation and diffusion-controlled mass transport,

whereas longer holding times further enhanced particle rearrangement, pore elimination, and microstructural consolidation after the liquid phase had formed. These results indicate that temperature played the dominant role in promoting densification, whereas holding time primarily contributed to further particle rearrangement and pore elimination after liquid-phase formation. Despite this improvement, the maximum relative density of 83.1% indicates that residual porosity remained under the pressureless sintering conditions evaluated. This incomplete densification may be associated with the limited sintering window explored (1380–1400 °C and 30–60 min) and with the initial powder packing and pore structure of the green compacts. Because the objective of this study was to compare the effect of CNT addition under identical processing conditions rather than to optimize the WC–Co matrix to near-theoretical density, no additional densification trials were performed. Further optimization of powder processing and sintering parameters will be required to achieve higher relative densities.

In the CNT-reinforced system, the slightly lower densification values may be associated with the presence of CNT-containing regions located at grain boundaries and interparticle regions. These carbonaceous structures may locally influence diffusion pathways and particle rearrangement during the early stages of liquid-phase sintering. However, despite this slight reduction in relative density, the CNT-containing samples maintained densification levels comparable to those of the unreinforced WC-Co system, indicating that the selected processing conditions were sufficient to achieve effective consolidation [10,14]. The densification behavior observed in Figure 2 suggests that the incorporation of CNTs did not drastically deteriorate the sintering response of the cemented carbide system. Instead, the slight reduction in relative density may reflect modifications in mass transport mechanisms during sintering, an effect that is further examined through the dilatometric analysis and activation energy evaluation presented in Sections 3.3 and 3.4. Furthermore, the controlled incorporation of CNTs may contribute to the development of a more homogeneous carbide distribution that becomes more evident in the subsequent microstructural and mechanical analyses.

3.2. Microstructural Evolution During Liquid-Phase Sintering

The densification behavior discussed in the previous section was closely associated with the microstructural evolution occurring during liquid-phase sintering. Figure 3 presents SEM micrographs of WC-Co cemented carbides processed under different sintering conditions. Although the representative SEM micrographs were acquired at different magnifications, the comparison focuses on qualitative microstructural features, including carbide distribution, residual porosity, particle rearrangement, and overall microstructural homogeneity. Significant changes in carbide morphology, particle rearrangement, and porosity distribution were observed as the sintering temperature and holding time increased.

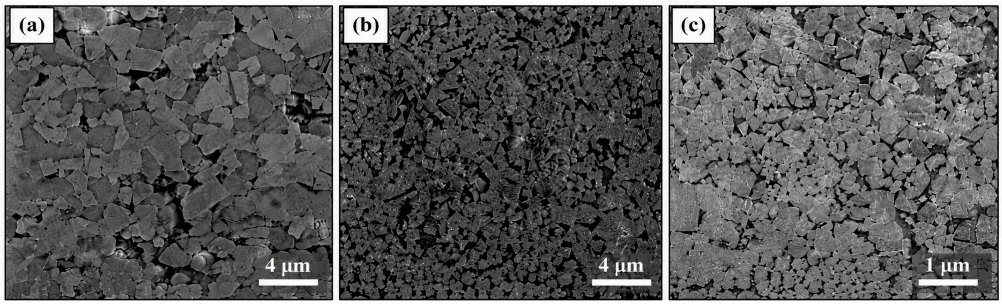


Figure 3. Representative SEM micrographs of WC-Co cemented carbides showing microstructural evolution under different liquid-phase sintering conditions: (**a**) 1380 °C for 30 min, (**b**) 1400 °C for 30 min, and (**c**) 1400 °C for 60 min.

At 1380 °C for 30 min (Figure 3a), the microstructure exhibited irregular carbide particle distribution accompanied by residual porosity and incomplete particle rearrangement. This behavior suggests that liquid-phase formation and diffusion-assisted transport mechanisms were still limited under these processing conditions. As the sintering temperature increased to 1400 °C for 30 min (Figure 3b), improved carbide rearrangement and partial pore elimination were observed, indicating enhanced liquid-phase-assisted densification. The reduction in porosity observed between Figure 3a,b is consistent with the increase in relative density from 71.3% to 76.4% reported in Figure 2. The microstructure obtained at 1400 °C for 60 min (Figure 3c) exhibited a more homogeneous carbide distribution and reduced porosity levels, suggesting that prolonged holding times promoted more effective dissolution–reprecipitation and mass transport mechanisms during sintering [25,33,34]. The higher degree of consolidation observed under these conditions is in agreement with the highest relative density value obtained for the WC-Co system (83.1%). Additionally, a more consolidated carbide network was observed as a consequence of enhanced diffusion kinetics and increased mobility of the cobalt-rich liquid phase [35]. The effect of CNT incorporation on the microstructural evolution of the cemented carbide systems is presented in Figure 4. In general, the CNT-reinforced samples exhibited a finer and more homogeneous carbide distribution compared with the unreinforced WC-Co systems, suggesting that CNT addition influenced the evolution of the microstructure during liquid-phase sintering.

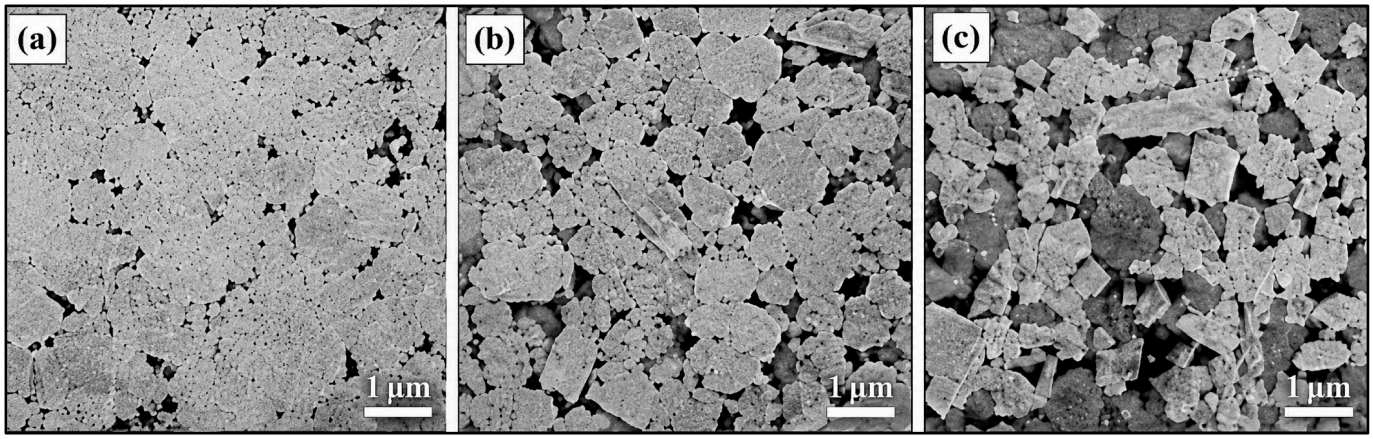


Figure 4. SEM micrographs of WC-Co reinforced with 5 vol.% CNT sintered under different liquid-phase sintering conditions showing the effect of CNT incorporation on microstructural evolution: (**a**) 1380 °C for 30 min, (**b**) 1400 °C for 30 min, and (**c**) 1400 °C for 60 min.

At 1380 °C for 30 min (Figure 4a), the CNT-reinforced microstructure showed the presence of fine carbide particles accompanied by residual porosity, indicating that the sintering process was still incomplete under these conditions. As the sintering temperature increased to 1400 °C for 30 min (Figure 4b), improved carbide rearrangement and enhanced densification were observed, together with a more homogeneous microstructural distribution. These observations are consistent with the densification behavior presented in Figure 2, where the relative density increased from 70.8% to 73.4%. The microstructure obtained at 1400 °C for 60 min (Figure 4c) revealed a more consolidated carbide network with reduced porosity and improved particle bonding. In addition, the microstructure in Figure 4c exhibits regions with different SEM contrast, where the light grey regions correspond to WC carbide particles, whereas the darker grey regions are associated with the cobalt-rich binder phase and interparticle regions. The increased visibility of these darker regions in Figure 4c is consistent with the more advanced stage of liquid-phase sintering achieved after prolonged holding, which resulted in improved particle rearrangement and microstructural consolidation. Since no local chemical analysis was performed, the phase

identification is based on the expected contrast of WC-Co cemented carbides observed by SEM. Furthermore, the CNT-containing samples exhibited a more homogeneous carbide distribution than the corresponding unreinforced WC-Co system processed under equivalent conditions. This behavior may be associated with the influence of CNT-derived carbonaceous regions on diffusion-controlled processes and local microstructural evolution during liquid-phase sintering [12,14,36,37]. The refined carbide distribution observed in the CNT-containing samples may contribute to the mechanical performance improvements discussed in subsequent sections, particularly in terms of fracture toughness. Moreover, the microstructural differences observed between WC-Co and WC-Co + 5 vol.% CNT suggest modifications in diffusion-controlled sintering mechanisms, an interpretation that is consistent with the activation energy results discussed later in Section 3.4.

3.3. Dilatometric Analysis and Densification Behavior

The densification behavior during liquid-phase sintering was further investigated through dilatometric analysis using different heating rates. Figures 5 and 6 present the relative density evolution of the WC-Co and WC-Co reinforced with 5 vol.% CNT systems, respectively, processed at heating rates of 5, 10, and 20 °C/min. Accordingly, Figures 5 and 6 present the complete recorded temperature ranges for the WC-Co and WC-Co + 5 vol.% CNT experimental series, respectively. The dilatometric behavior of the unreinforced WC-Co system (Figure 5) revealed characteristic densification stages associated with liquid-phase sintering. Initially, a slight reduction in relative density was observed as temperature increased, which may be attributed to thermal expansion effects and particle rearrangement occurring during the early heating stages. As the temperature approached the liquid-phase formation region, a pronounced densification process occurred, characterized by a rapid increase in relative density.

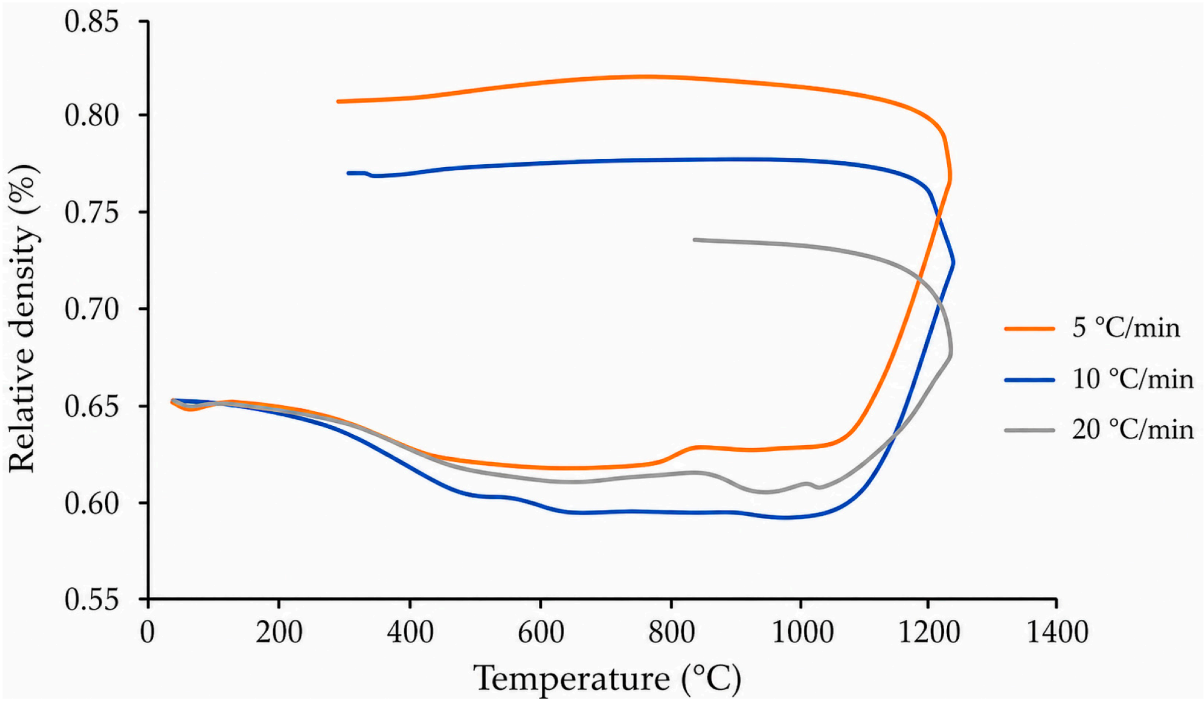


Figure 5. Relative density evolution obtained by dilatometric analysis of WC-Co cemented carbides processed at heating rates of 5, 10, and 20 °C/min up to 1260 °C.

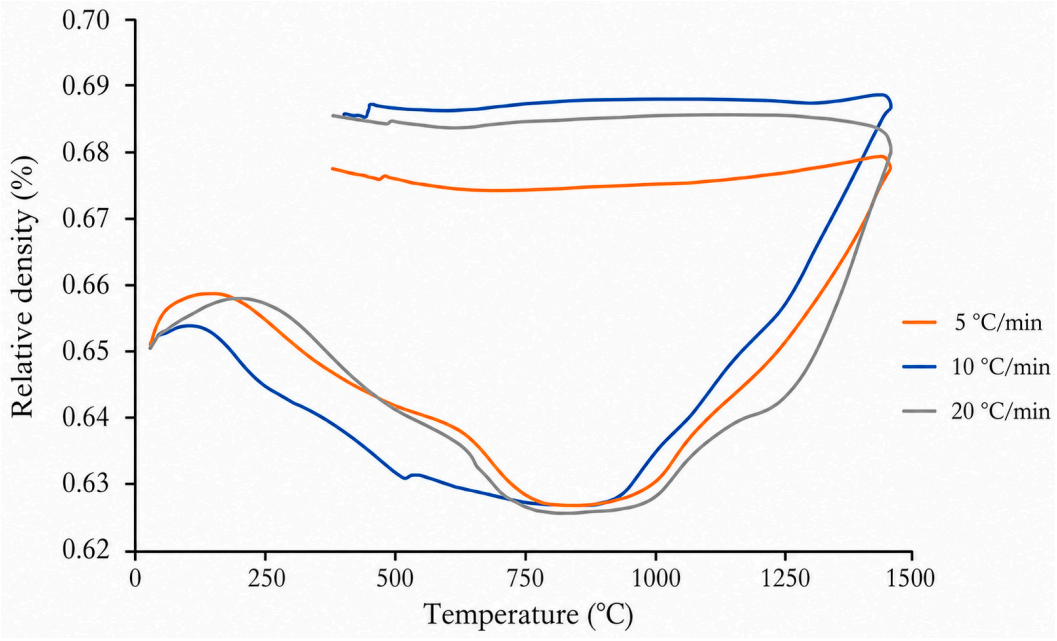


Figure 6. Relative density evolution obtained by dilatometric analysis of WC-Co reinforced with 5 vol.% CNT processed at heating rates of 5, 10, and 20 °C/min up to 1420 °C.

The samples processed at lower heating rates exhibited higher final densification levels compared with those processed at faster heating rates. In particular, the specimen heated at 5 °C/min reached the highest relative density values, suggesting that slower heating rates promoted enhanced diffusion and more effective liquid-phase-assisted particle rearrangement. Conversely, the samples processed at 20 °C/min showed comparatively lower densification, indicating that rapid heating restricted the time available for diffusion-controlled mass transport mechanisms during sintering [34,38]. Additionally, the onset of rapid densification shifted depending on the heating rate, indicating a strong kinetic dependence of the sintering process. This behavior suggests that heating rate directly influences liquid-phase activation, pore elimination, and particle rearrangement mechanisms in WC-Co cemented carbides [25,39]. The dilatometric response of the WC-Co reinforced with 5 vol.% CNT system is presented in Figure 6. Similar densification stages were observed; however, noticeable differences in densification behavior were identified compared with the unreinforced WC-Co system. The CNT-containing samples exhibited a more gradual densification response, suggesting that CNT incorporation modified the diffusion-controlled mass transport mechanisms operating during liquid-phase sintering.

Compared with the unreinforced WC-Co system, the CNT-reinforced specimens exhibited a broader and more gradual densification response over a wider temperature interval. Although measurable dimensional changes became apparent at lower temperatures, the subsequent densification proceeded more progressively, indicating that CNT incorporation modified the diffusion-controlled mass transport mechanisms governing liquid-phase sintering. This behavior suggests that the presence of CNT-containing regions altered the sequence of particle rearrangement and diffusion processes during heating, resulting in a more distributed densification process rather than the abrupt densification observed in the unreinforced WC-Co system [14,36,40,41]. This interpretation is consistent with the higher apparent activation energy obtained for the CNT-reinforced material, indicating that although densification initiated progressively over a broader temperature range, greater energy was required to achieve final consolidation. These observations are consistent with the slightly lower relative density values reported in Figure 2 and with the more homogeneous carbide distributions observed in Figure 4. Unlike the unreinforced WC-Co system,

the CNT-containing samples exhibited smaller differences in final densification behavior among the evaluated heating rates. Overall, the dilatometric analysis demonstrated that both heating rate and CNT incorporation strongly influenced the densification behavior and liquid-phase sintering response of the studied cemented carbide systems. These results provide a direct basis for the activation energy analysis presented in the following section, where the influence of CNT addition on the apparent activation energy of densification is quantitatively evaluated.

3.4. Activation Energy Analysis

The apparent activation energy associated with the densification process was estimated from the dilatometric data using a non-isothermal kinetic approach based on constant heating-rate experiments. For this analysis, the Arrhenius-type relationship was considered according to:

$$ln\left[T\left(\frac{d\delta}{dt}\right)\dot{T}\right] = -\frac{Q}{RT} + C \quad (1)$$

where T is the absolute temperature, $\frac{d\delta}{dt}$ is the densification rate, $\dot{T}$ is the heating rate, Q is the apparent activation energy, R is the universal gas constant, and C is a constant. Therefore, the apparent activation energy was estimated from the slope of the linear relationship between $ln\left[T\left(\frac{d\delta}{dt}\right)\dot{T}\right]$ and $1/T$ [42,43].

As shown in Figure 7, the Arrhenius plot obtained for the unreinforced WC-Co system yielded an apparent activation energy of 99.36 ± 8 kJ/mol. The calculated apparent activation energy was 99.36 ± 8 kJ/mol, indicating that densification under the evaluated conditions was governed by thermally activated mass transport mechanisms associated with liquid-phase sintering. This value is consistent with the complex nature of WC-Co sintering, where particle rearrangement, dissolution–reprecipitation phenomena, liquid-phase formation, and diffusion-assisted transport may contribute simultaneously to densification [31,39,44].

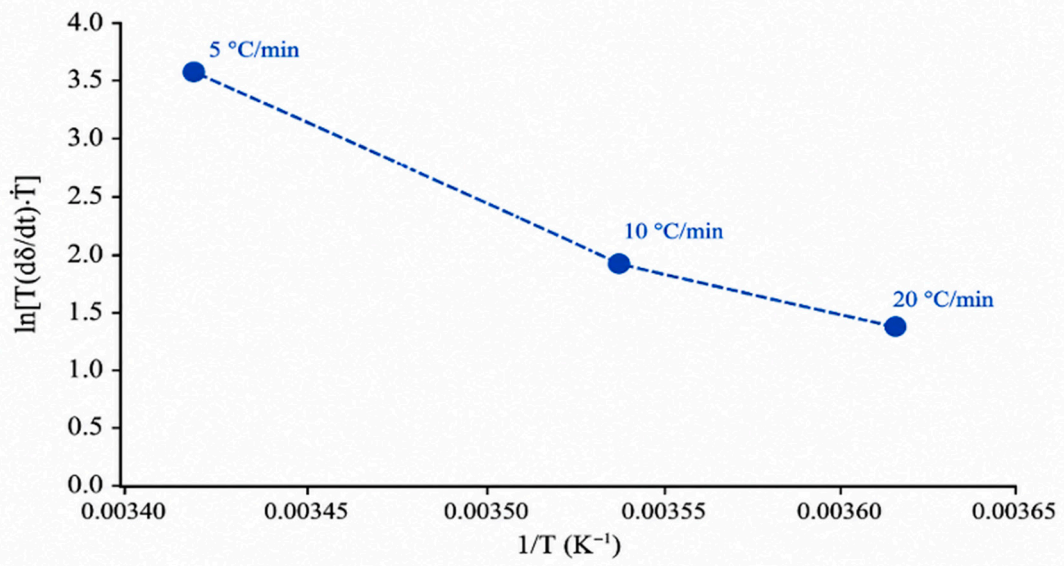


Figure 7. Arrhenius plot for WC-Co powders obtained from dilatometric data at heating rates of 5, 10, and 20 °C/min.

For the WC-Co reinforced with 5 vol.% CNT system, the Arrhenius plot is shown in Figure 8. In this case, the apparent activation energy increased to 126.47 kJ/mol. Compared with the unreinforced WC-Co system, CNT incorporation increased the apparent activation energy by approximately 27%, indicating that additional energy was required to activate

the densification mechanisms operating during liquid-phase sintering. The increase in apparent activation energy suggests that CNT incorporation modified the diffusion-controlled processes governing densification. This interpretation is consistent with the dilatometric behavior discussed in Section 3.3, where the CNT-containing samples exhibited a broader and more gradual densification response over a wider temperature range. The higher activation energy requirement may reflect modifications in local mass transport pathways and particle rearrangement mechanisms introduced by CNT addition [14,36,40,41]. The apparent increase in activation energy is also consistent with the microstructural observations presented in Figure 4. Although the CNT-containing samples exhibited slightly lower relative density values than the unreinforced WC-Co system, they developed a comparatively finer and more homogeneous carbide distribution. These results suggest that CNT addition altered the kinetics of microstructural evolution during liquid-phase sintering, leading to a modified balance between densification and microstructural coarsening. It is important to note that the calculated activation energies should be interpreted as apparent values, since liquid-phase sintering of WC-Co involves multiple overlapping mechanisms rather than a single diffusion-controlled process. Nevertheless, the substantial increase in activation energy observed after CNT incorporation provides strong evidence that CNT addition significantly influences the densification pathway of WC-Co cemented carbides.

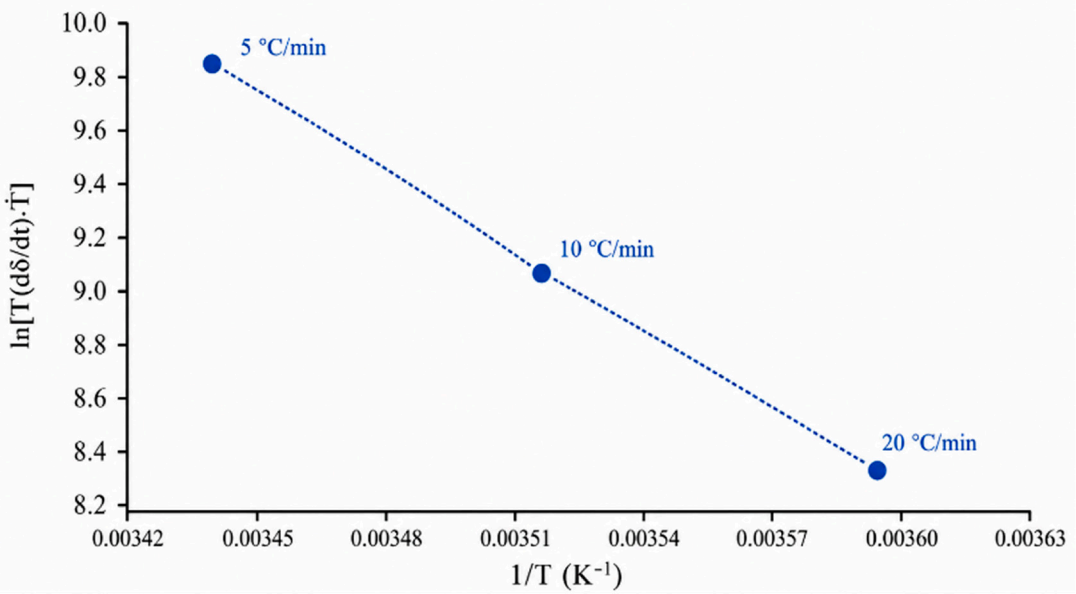


Figure 8. Arrhenius plot for WC-Co + 5 vol.% CNT powders obtained from dilatometric data at heating rates of 5, 10, and 20 °C/min.

Furthermore, the higher activation energy associated with the CNT-containing system may contribute to the improved fracture resistance discussed in the following section. The combination of modified densification kinetics, more homogeneous carbide distributions, and altered mass transport behavior suggests that CNTs act not only as a reinforcing phase but also as microstructural and kinetic modifiers during liquid-phase sintering.

3.5. Mechanical Behavior

The mechanical performance of the investigated cemented carbide systems was evaluated through Vickers hardness and fracture toughness measurements, as shown in Figure 9. The results revealed that the incorporation of 5 vol.% CNT improved the overall mechanical response of the WC-Co system. The unreinforced WC-Co specimen exhibited a hardness of approximately 995 kgf/mm^2 and a fracture toughness of 8.6 MPa·m$^{1/2}$, whereas the

CNT-reinforced material reached values close to 1090 kgf/mm^2 and 10.5 MPa·m$^{1/2}$, respectively. In addition, the reinforced sample exhibited a fracture toughness higher than that measured for the commercial WC-Co reference material (9.6 MPa·m$^{1/2}$), indicating that CNT incorporation contributed not only to hardness enhancement but also to improved resistance against crack propagation. The simultaneous increase in hardness and fracture toughness is particularly relevant because these properties often exhibit a competitive relationship in cemented carbides [40,41,45]. The improved mechanical response observed in the CNT-containing material may be associated with the modified microstructural evolution occurring during liquid-phase sintering. As discussed in Section 3.2, the addition of CNTs promoted a finer and more homogeneous carbide distribution compared with the unreinforced WC-Co system. Such microstructural characteristics are commonly associated with improved resistance to localized deformation and more uniform stress distribution during crack initiation and propagation [12,14,46,47]. The densification and activation energy analyses presented in Sections 3.3 and 3.4 further support the observed mechanical behavior. Although the CNT-containing specimens exhibited slightly lower relative density values than the unreinforced WC-Co system, they showed a higher apparent activation energy (126.47 kJ/mol versus 99.36 ± 8 kJ/mol). This increase suggests that CNT incorporation modified the diffusion-controlled processes governing densification and microstructural evolution during liquid-phase sintering. The resulting microstructure appears to favor improved mechanical performance despite the slight reduction in final densification. Previous studies on CNT-reinforced WC-Co cemented carbides have primarily focused on the influence of CNT incorporation on microstructural refinement and the resulting improvements in hardness and fracture toughness [12–16]. The present study is consistent with those observations while providing additional insight into the mechanisms governing these improvements. By combining dilatometric analysis, activation energy evaluation, microstructural characterization, densification measurements, and mechanical testing under identical liquid-phase sintering conditions, this work establishes a direct relationship between CNT incorporation, densification kinetics, microstructural evolution, and mechanical performance. This integrated experimental approach provides a more comprehensive understanding of the role of CNTs during liquid-phase sintering of WC-Co cemented carbides.

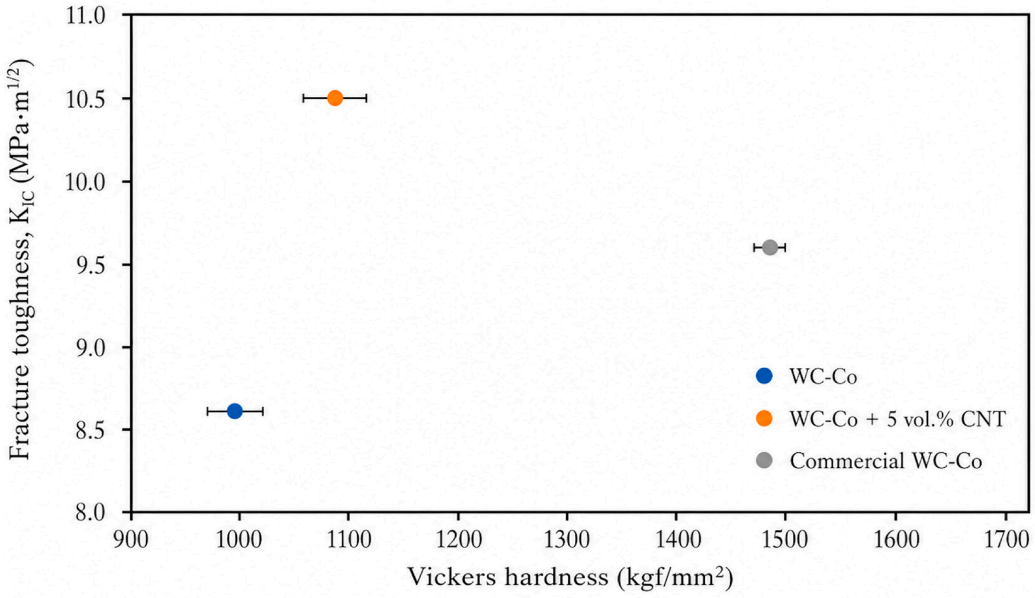


Figure 9. Vickers hardness and fracture toughness of WC-Co, WC-Co + 5 vol. % CNT, and commercial WC-Co sintered at 1400 °C for 60 min.

Compared with the commercial WC-Co reference material, the lower hardness obtained in the CNT-reinforced specimen is consistent with its lower relative density achieved under the investigated sintering conditions. The maximum relative density obtained in the CNT-reinforced material (82.2%) remained below that typically achieved in fully consolidated commercial cemented carbides, and the presence of residual porosity is known to reduce hardness. Nevertheless, the refined and more homogeneous carbide distribution together with the modified microstructural evolution promoted by CNT incorporation contributed to superior fracture toughness observed for the CNT-reinforced material, indicating that the present processing route favored crack-growth resistance rather than maximum hardness. It should be noted that the WC grain size was not quantitatively measured in either the sintered specimens or the commercial WC-Co reference material. Therefore, the interpretation presented above is based on the experimentally evaluated parameters, including relative density, residual porosity, microstructural evolution, and CNT incorporation, while the possible contribution of WC grain size could not be independently assessed in the present study.

Additional evidence of the enhanced fracture resistance is provided in Figure 10. The SEM micrographs show the crack propagation behavior after Vickers indentation in the CNT-reinforced material. Previous measurements performed on the investigated systems indicated that the average crack length decreased from approximately 72.1 μm in WC-Co to 62.6 μm in the CNT-reinforced material.

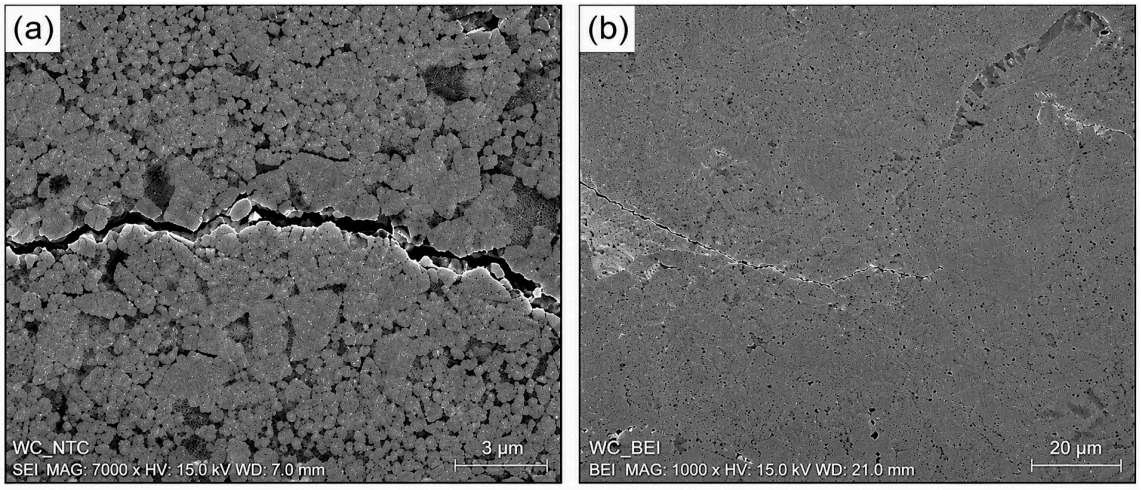


Figure 10. SEM micrographs of WC-Co + 5 vol.% CNT showing crack propagation behavior after Vickers indentation at different magnifications: (**a**) high-magnification SEM image; (**b**) low-magnification SEM image.

The shorter crack propagation distance is consistent with the higher fracture toughness values obtained for the reinforced material and indicates an increased resistance to crack growth [27,45,48]. These observations suggest that the refined carbide distribution and modified sintering behavior promoted by CNT incorporation contributed to restricting crack propagation and improving damage tolerance [46,48,49].

Figure 11 provides further insight into the fractured microstructure of the WC-Co + 5 vol.% CNT system. Filamentous features were observed between carbide particles at different magnifications. These features remained identifiable after liquid-phase sintering at 1400 °C for 60 min, suggesting that part of the carbonaceous reinforcement remained distributed within the fractured microstructure after processing. Although the present observations do not allow a direct determination of the contribution of individual CNTs to fracture resistance, the presence of these filamentous regions is consistent with the improved fracture toughness and reduced crack

propagation distances observed in Figures 9 and 10. Similar observations have been reported in CNT-reinforced ceramic and metal-matrix systems, where carbon nanotubes contribute to toughening mechanisms through crack deflection, load transfer, and energy dissipation during fracture [50,51]. Overall, the results demonstrate that CNT incorporation produced a beneficial combination of increased hardness, improved fracture toughness, and enhanced resistance to crack propagation. The observed mechanical improvements were closely associated with the modified densification behavior, increased activation energy, more homogeneous carbide distributions, and the presence of filamentous CNT-containing regions observed within the fractured microstructure. These findings indicate that CNT addition represents an effective strategy for enhancing the performance of WC-Co cemented carbides processed by liquid-phase sintering.

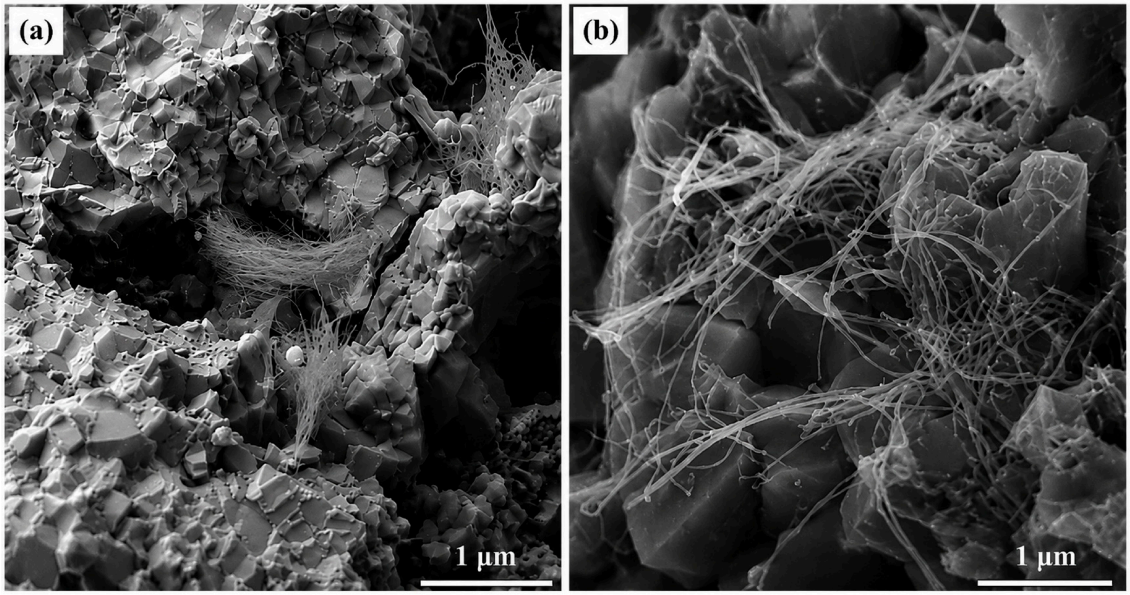


Figure 11. SEM micrographs of the fracture surface of WC-Co + 5 vol.% CNT sintered at 1400 °C for 60 min at different magnifications: (**a**) low-magnification view showing filamentous features on the fracture surface; (**b**) high-magnification view highlighting the filamentous structures between carbides particles.

4. Conclusions

The effect of 5 vol.% carbon nanotube (CNT) addition on the densification behavior, microstructural evolution, sintering kinetics, activation energy, and mechanical performance of WC-Co cemented carbides processed by liquid-phase sintering was systematically investigated. For both WC-Co and WC-Co + 5 vol.% CNT systems, relative density increased with increasing sintering temperature and holding time, indicating progressive consolidation through liquid-phase-assisted densification mechanisms. Although the CNT-containing samples exhibited slightly lower relative density values than the unreinforced WC-Co specimens, effective densification was achieved under all evaluated processing conditions. Simultaneously, the incorporation of CNTs promoted a more homogeneous carbide distribution together with a reduction in residual porosity, demonstrating that CNT addition influenced the microstructural evolution occurring during sintering.

Dilatometric analysis revealed that both heating rate and CNT incorporation significantly affected the densification response of the investigated systems. The CNT-reinforced materials exhibited a broader and more gradual densification behavior over a wider temperature range compared with the unreinforced WC-Co system. This behavior was reflected in the apparent activation energy values, which increased from 99.36 ± 8 kJ/mol for WC-Co to 126.47 kJ/mol for WC-Co + 5 vol.% CNT, corresponding to an increase of approximately

27%. This substantial increase provides quantitative evidence that CNT incorporation modified the densification pathway and altered the diffusion-controlled kinetic processes governing liquid-phase sintering. The combined dilatometric, microstructural, and activation energy analyses indicate that CNT addition acts as an effective modifier of mass transport mechanisms during consolidation.

The modified densification behavior and microstructural evolution were directly reflected in the mechanical performance of the investigated materials. The CNT-reinforced system achieved hardness and fracture toughness values of approximately 1090 kgf/mm^2 and 10.5 MPa·m$^{1/2}$, respectively, exceeding those of the unreinforced WC-Co system and exhibiting fracture toughness superior to that of the commercial WC-Co reference material. Furthermore, the reduced crack propagation length observed after Vickers indentation, together with the filamentous features observed within the fractured microstructure, supported the enhanced resistance to crack growth promoted by CNT incorporation. Overall, the results demonstrate that CNTs function not only as a reinforcing phase but also as microstructural and kinetic modifiers during liquid-phase sintering, providing an effective strategy for tailoring densification behavior, modifying microstructural evolution, and improving the mechanical performance of WC-Co cemented carbides.

Author Contributions: J.L.C.-V.: Conceptualization, methodology, formal analysis, data curation, visualization, writing—original draft preparation, writing—review and editing, and project administration. G.C.-S.: Investigation and data curation. V.S.L.-Á.: Validation. J.L.-R.: Conceptualization, methodology, supervision, project administration, writing—review and editing, and funding acquisition. All authors have read and agreed to the published version of the manuscript.

Funding: This research was financially supported by the Coordinación de la Investigación Científica (CIC) of the Universidad Michoacana de San Nicolás de Hidalgo (UMSNH) and by the Secretaría de Ciencia, Humanidades, Tecnología e Innovación (SECIHTI) through a postdoctoral fellowship awarded to CVU 511121.

Data Availability Statement: The original contributions presented in this study are included in the article. Further inquiries can be directed to the corresponding author.

Conflicts of Interest: The authors declare no conflicts of interest. The sponsors had no role in the design, execution, interpretation, or writing of the study.

References

1. Straumal, B.B.; Konyashin, I. WC-Based Cemented Carbides with High Entropy Alloyed Binders: A Review. *Metals* **2023**, *13*, 171. [CrossRef]
2. Kawakami, M. Cemented Carbide Tools and Moulds for Wear-Resistant Applications in Japan. *Int. J. Refract. Met. Hard Mater.* **2024**, *118*, 106477. [CrossRef]
3. Pittari, J.J., III; Swab, J.J.; Wright, J.; Atwater, K. Mechanical Evaluation of WC-Co Materials with Varying Microstructures. *Int. J. Refract. Met. Hard Mater.* **2022**, *104*, 105809. [CrossRef]
4. González Oliver, C.J.R.; Alvarez, E.A.; García, J.L. Kinetics of Densification and Grain Growth in Ultrafine WC-Co Composites. *Int. J. Refract. Met. Hard Mater.* **2016**, *59*, 121–131. [CrossRef]
5. Sadangi, R.; Bose, A. Some Aspects of Solid Solution Grain Growth Inhibitors in Cemented Tungsten Carbides. *Int. J. Refract. Met. Hard Mater.* **2024**, *119*, 106474. [CrossRef]
6. Müller, D.; Konyashin, I.; Farag, S.; Ries, B.; Zaitsev, A.A.; Loginov, P.A. WC Coarsening in Cemented Carbides during Sintering. Part I: The Influence of WC Grain Size and Grain Size Distribution. *Int. J. Refract. Met. Hard Mater.* **2022**, *102*, 105714. [CrossRef]
7. Yu, S.; Min, F.; Ying, G.; Noudem, J.G.; Liu, S.; Zhang, J. The Grain Growth and Boundary Evolution of Extra-Coarse-Grained Cemented Carbides by Pressureless Sintering of Ball-Milling-Mixed WC with Co at Different Temperature. *Mater. Charact.* **2021**, *181*, 111386. [CrossRef]
8. He, R.; Yang, Q.; Li, B.; Lou, J.; Yang, H.; Ruan, J. Grain Growth Behaviour and Mechanical Properties of Coarse-Grained Cemented Carbides with Bimodal Grain Size Distributions. *Mater. Sci. Eng. A* **2021**, *805*, 140586. [CrossRef]

9. Konyashin, I.; Nazari, N.; Mueller, D.; Farag, S.; Ries, B.; Bondarev, A.; Meledin, A. WC Coarsening in Cemented Carbides during Sintering. Part II: Mechanisms of the Influence of Different Grain Growth Inhibitors. *Int. J. Refract. Met. Hard Mater.* **2025**, *128*, 107087. [CrossRef]
10. Zhang, S.; Su, W.; Sun, L.; Wang, J. Effect of Carbon Nanotubes Additives on Mechanical Properties of WC–6Co Cemented Carbide. *Int. J. Appl. Ceram. Technol.* **2023**, *20*, 1318–1327. [CrossRef]
11. Jiang, H.; Zhao, Z.; Qian, Y.; Yan, Y.; Lei, Y.; Zhang, Z.; Zhang, S.; Chen, Z.; Wang, S.; Lu, X. Effects of Nanocomposite Grain Growth Inhibitors and Multi-Walled Carbon Nanotubes on the Microstructure and Mechanical Properties of Ultrafine Cemented Carbides. *J. Mater. Res. Technol.* **2023**, *26*, 3054–3069. [CrossRef]
12. Jiang, J.; Ouyang, S.; Chen, H.; Guo, S.; Yin, L.; Tan, Z.; Shi, H.; Zhong, Z.; Qiu, L. Effect of MWCNTs on Microstructure and Properties of WC-9Co Gradient Cemented Carbides. *Ceram. Int.* **2022**, *48*, 19295–19304. [CrossRef]
13. Shi, X.L.; Yang, H.; Wang, S.; Shao, G.; Duan, X. Fabrication and Properties of WC–10Co Cemented Carbide Reinforced by Multi-Walled Carbon Nanotubes. *Mater. Sci. Eng. A* **2008**, *486*, 489–495. [CrossRef]
14. Zhang, L.; Wang, Y.; Yang, Y.; Li, S. In Situ Growth of Carbon Nanotubes on WC-Co Powder for Toughening Cemented Carbide by Different Consolidation Strategies. *J. Am. Ceram. Soc.* **2025**, *108*, e20607. [CrossRef]
15. Kuai, J.; Zhang, H.; Ardashev, D.V.; Li, X.; Liu, S. Mechanical Properties of WC-10Co-CNT Nano-Cemented Carbide. *Ferroelectrics* **2022**, *593*, 181–187. [CrossRef]
16. Wang, D.; Liu, S.; He, L.; Kan, S.; Zhou, X.; Ren, Z.; Ma, B.; Yang, Y. In-situ Preparation of CNTs/WC-CoCr Powder and Their HVAF Coatings: Microstructure and Mechanical Properties. *Int. J. Refract. Met. Hard Mater.* **2026**, *134*, 107496. [CrossRef]
17. Sun, Y.; Su, W.; Yang, H.; Ruan, J. Effects of WC Particle Size on Sintering Behavior and Mechanical Properties of Coarse-Grained WC–8Co Cemented Carbides Fabricated by Unmilled Composite Powders. *Ceram. Int.* **2015**, *41*, 14482–14491. [CrossRef]
18. Muñoz-Ortuño, L.; Soria-Biurrun, T.; Vornberger, A.; Pötschke, J.; Ronkainen, J.; Karhumaa, T.; Sánchez-Moreno, J.M. Effect of Powder Characteristics on Shrinkage Kinetics of WC-Co-Cr Zn-Reclaimed Submicron Powders. *Int. J. Refract. Met. Hard Mater.* **2026**, *136*, 107603. [CrossRef]
19. Lantcev, E.; Nokhrin, A.; Malekhonova, N.; Boldin, M.; Chuvil'deev, V.; Blagoveshchenskiy, Y.; Isaeva, N.; Andreev, P.; Smetanina, K.; Murashov, A. A Study of the Impact of Graphite on the Kinetics of SPS in Nano- and Submicron WC-10%Co Powder Compositions. *Ceramics* **2021**, *4*, 331–363. [CrossRef]
20. Pérez Gasquez y Marín, A.; López-Tinoco, J.; Lara-Romero, J.; Rangel-Segura, R.; Huirache-Acuña, R.; Stacchiola, D. Influence of Carrier Gas Flow Rate on the Synthesis of Long MWCNTs from Biorenewable Carbon Feedstock: α-Pinene. *Beilstein Arch.* **2026**, *2026*, 11. [CrossRef]
21. Lara-Romero, J.; Calva-Yáñez, J.C.; López-Tinoco, J.; Alonso-Núñez, G.; Jiménez-Sandoval, S.; Paraguay-Delgado, F. Temperature Effect on the Synthesis of Multi-Walled Carbon Nanotubes by Spray Pyrolysis of Botanical Carbon Feedstocks: Turpentine, α-Pinene and β-Pinene. *Fuller. Nanotub. Carbon Nanostruct.* **2011**, *19*, 483–496. [CrossRef]
22. Osorio, A.G.; Silveira, I.C.L.; Bueno, V.L.; Bergmann, C.P. H2SO4/HNO3/HCl—Functionalization and Its Effect on Dispersion of Carbon Nanotubes in Aqueous Media. *Appl. Surf. Sci.* **2008**, *255*, 2485–2489. [CrossRef]
23. Sezer, N.; Koç, M. Oxidative Acid Treatment of Carbon Nanotubes. *Surf. Interfaces* **2019**, *14*, 1–8. [CrossRef]
24. Soni, S.K.; Tody, V.; Thomas, B. Influence of Dispersion Technique/Time on Dispersion Stability, Aspect Ratio and Morphology of Multi-Walled Carbon Nanotubes. *Int. J. Nanotechnol.* **2021**, *18*, 590–609. [CrossRef]
25. Niu, Y.; Gong, P.; Xu, X.; Wang, X.; Ma, Y.; Li, M.; Lu, Q.; Yang, H.; Liu, Z.; Zhang, M.; et al. Preparation of WC-Co Cemented Carbide by Spark Plasma Sintering: Microstructure Evolution, Mechanical Properties and Densification Mechanism. *Int. J. Refract. Met. Hard Mater.* **2025**, *126*, 106964. [CrossRef]
26. Oliver, C.; Schuh, C.A. Kissinger-Style Kinetic Analysis for Sintering Dilatometry Data. *Metall. Mater. Trans. A* **2021**, *52*, 4479–4487. [CrossRef]
27. Lu, Z.; Du, J.; Sun, Y.; Su, G.; Zhang, C.; Kong, X. Effect of Ultrafine WC Contents on the Microstructures, Mechanical Properties and Wear Resistances of Regenerated Coarse Grained WC-10Co Cemented Carbides. *Int. J. Refract. Met. Hard Mater.* **2021**, *97*, 105516. [CrossRef]
28. Ponton, C.B.; Rawlings, R.D. Vickers Indentation Fracture Toughness Test Part 1: Review of Literature and Formulation of Standardised Indentation Toughness Equations. *Mater. Sci. Technol.* **1989**, *5*, 865–872. [CrossRef]
29. Žmak, I.; Ćorić, D.; Mandić, V.; Ćurković, L. Hardness and Indentation Fracture Toughness of Slip Cast Alumina and Alumina-Zirconia Ceramics. *Materials* **2020**, *13*, 122. [CrossRef] [PubMed]
30. Nie, H.; Zhang, T. Development of Manufacturing Technology on WC–Co Hardmetals. *Tungsten* **2019**, *1*, 198–212. [CrossRef]
31. Ju, J.; Huang, D.; Xu, H.; Dong, D.; Lou, J.; Xu, Y.; Shi, J.; Zhu, L. Effects of Sintering Pressure and Co Content on the Microstructure and Mechanical Performance of WC–Co Cemented Carbides. *Metals* **2025**, *15*, 930. [CrossRef]
32. Roulon, Z. Effect of Binder on Sintering and Microstructure of Cemented Carbides. Ph.D. Thesis, Université Grenoble Alpes, Grenoble, France, 2019.

33. Zhang, J.; Li, K.; Chen, Y.; Qian, C.; Zhang, S.; Cheng, H. Interplay of Carbon Content and Sintering Temperature on Microstructure and Mechanical Behavior in Ultrafine-Grained WC-10CoNiFe and WC-10Co Cemented Carbides. *Materials* **2025**, *18*, 2789. [CrossRef] [PubMed]
34. Lantsev, E.A.; Chuvil'deev, V.N.; Nokhrin, A.V.; Boldin, M.S.; Malekhonova, N.V.; Blagoveshchenskii, Y.V.; Isaeva, N.V.; Tsvetkov, Y.V.; Andreev, P.V.; Smetanina, K.E. Study of the Kinetics of Spark Plasma Sintering of Ultrafine-Grained Hard Alloys WC–10%Co. *J. Phys. Conf. Ser.* **2020**, *1431*, 012030. [CrossRef]
35. Emanuelli, L.; Molinari, A.; Arrighetti, G.; Garoli, G. Effect of the sintering parameters on the liquid Co migration in WC-Co. *Int. J. Refract. Met. Hard Mater.* **2018**, *70*, 202–209. [CrossRef]
36. Zhang, F.; Shen, J.; Sun, J. Processing and Properties of Carbon Nanotubes–Nano-WC-Co Composites. *Mater. Sci. Eng. A* **2004**, *381*, 86–91. [CrossRef]
37. Bai, T.; Xie, T. Influence of TiO_2 Contents and Sintering Temperature on the Microstructure and Mechanical Properties of WC-Al_2O_3 Cemented Carbide Reinforced by Multi-Wall Carbon Nanotubes. *J. Alloys Compd.* **2018**, *745*, 562–568. [CrossRef]
38. Lantsev, E.A.; Chuvil'deev, V.N.; Nokhrin, A.V.; Boldin, M.S.; Malekhonova, N.V.; Blagoveshchenskii, Y.V.; Isaeva, N.V.; Tsvetkov, Y.V.; Andreev, P.V.; Smetanina, K.E. Kinetics of Spark Plasma Sintering of WC–10% Co Ultrafine-Grained Hard Alloy. *Inorg. Mater. Appl. Res.* **2020**, *11*, 586–597. [CrossRef]
39. Roulon, Z.; Missiaen, J.-M.; Lay, S. Shrinkage and Microstructure Evolution during Sintering of Cemented Carbides with Alternative Binders. *Int. J. Refract. Met. Hard Mater.* **2021**, *101*, 105665. [CrossRef]
40. Zhang, F.M.; Sun, J.F.; Shen, J. Effects of Carbon Nanotubes Incorporation on the Grain Growth and Properties of WC/Co Nanocomposites. *Mater. Sci. Forum* **2005**, *475–479*, 989–992. [CrossRef]
41. Tan, G.-L.; Wu, X.-J.; Li, Z.-Q. Carbon Nanotubes Strengthened Nanophase WC-Co Hard Alloys. *Adv. Eng. Mater.* **2006**, *8*, 62–72. [CrossRef]
42. Kim, S.H.; Kim, D.-G.; Park, M.S.; Seo, Y.I.; Kim, Y.D. Sintering Kinetics Analysis of Molybdenum Nanopowder in a Non-Isothermal Process. *Met. Mater. Int.* **2011**, *17*, 63–66. [CrossRef]
43. Garcia-Carrillo, A.M.; Lemus-Ruiz, J.; Olmos, L. Sintering Analysis of CoCrMo Powders by In-Situ Dilatometry. *Mater. Res.* **2024**, *27*, e20240286. [CrossRef]
44. Buravleva, A.A.; Fedorets, A.N.; Vornovskikh, A.A.; Ognev, A.V.; Nepomnyushchaya, V.A.; Sakhnevich, V.N.; Lembikov, A.O.; Kornakova, Z.E.; Kapustina, O.V.; Tarabanova, A.E.; et al. Spark Plasma Sintering of WC-Based 10wt%Co Hard Alloy: A Study of Sintering Kinetics and Solid-Phase Processes. *Materials* **2022**, *15*, 1091. [CrossRef] [PubMed]
45. Lu, Z.; Wang, W.; Zeng, M.; Zhu, M. Breaking the Hardness–Toughness Trade-Off in WC–Co Hardmetals: Introduction of Dual-Scale Plate-Like WC and Modification of Prediction Models. *Int. J. Refract. Met. Hard Mater.* **2022**, *109*, 105910. [CrossRef]
46. Ma, M.; Diao, Y.; Lu, Z.; Huang, Q.; Wang, K.; Li, G.; Wang, Q. Interface Regulation of Nanocrystalline WC-10Co Cemented Carbides for Enhanced Hardness and Fracture Toughness Balance. *J. Alloys Compd.* **2025**, *1040*, 183708. [CrossRef]
47. Li, D.; Liu, Y.; Ye, J.; Chen, X.; Wang, L. The enhancement of the microstructure and mechanical performances of ultrafine WC-Co cemented carbides by optimizing Cr2(C,N) addition and WC particle sizes. *Int. J. Refract. Met. Hard Mater.* **2021**, *98*, 105518. [CrossRef]
48. Xu, M.; Wang, H.; Liu, X.; Lu, H.; Song, X. Microstructural Evolution and Toughening Mechanism of WC-Co Composite Prepared by Amorphous-Crystallization Method. *Mater. Res. Lett.* **2024**, *12*, 921–928. [CrossRef]
49. Fooladi Mahani, S.; Liu, C.; Lin, L.L.; Ramírez, G.; Wen, X.; Llanes, L. Damage Tolerance and Residual Fatigue Strength/Life of WC-Co Cemented Carbides. *Int. J. Refract. Met. Hard Mater.* **2025**, *129*, 107117. [CrossRef]
50. Chan, K.F.; Zaid, M.H.M.; Mamat, M.S.; Liza, S.; Tanemura, M.; Yaakob, Y. Recent Developments in Carbon Nanotubes-Reinforced Ceramic Matrix Composites: A Review on Dispersion and Densification Techniques. *Crystals* **2021**, *11*, 457. [CrossRef]
51. Almansoori, A.; Balázsi, K.; Balázsi, C. Advances, Challenges, and Applications of Graphene and Carbon Nanotube-Reinforced Engineering Ceramics. *Nanomaterials* **2024**, *14*, 1881. [CrossRef] [PubMed]

Disclaimer/Publisher's Note: The statements, opinions and data contained in all publications are solely those of the individual author(s) and contributor(s) and not of MDPI and/or the editor(s). MDPI and/or the editor(s) disclaim responsibility for any injury to people or property resulting from any ideas, methods, instructions or products referred to in the content.